Zhao et al. Advances in Bridge Engineering (2021) 2:5
https://doi.org/10.1186/s43251-020-00026-3

Advances in Bridge Engineering

ORIGINAL INNOVATION Open Access

An accurate frequency-domain model of water interaction with cylinders of arbitrary shape during earthquakes

Mi Zhao, Xiaojing Wang, Piguang Wang*, Chao Zhang and Xiuli Du

* Correspondence:
wangpiguang1985@126.com
Key Laboratory of Urban Security and Disaster Engineering of Ministry of Education, Beijing University of Technology, Beijing 100124, China

Abstract

An accurate frequency domain model is proposed to analyze the seismic response of uniform vertical cylinders with arbitrary cross section surrounded by water. According to the boundary conditions and using the variables separation method, the vertical modes of the hydrodynamic pressure are firstly obtained. Secondly, the three-dimensional wave equation can be simplified to a two-dimensional Helmholtz equation. Introducing the scaled boundary coordinate, a scaled boundary finite element (SBFE) equation which is a linear non-homogeneous second-order ordinary equation is derived by weighted residual method. The dynamic-stiffness matrix equation for the problem is furtherly derived. The continued fraction is acted as the solution of the dynamic-stiffness matrix for cylinder dynamic interaction of cylinder with infinite water. The coefficient matrices of the continued fraction are derived recursively from the SBFE equation of dynamic-stiffness. The accuracy of the present method is verified by comparing the hydrodynamic force on circular, elliptical and rectangle cylinders with the analytical or numerical solutions. Finally, the proposed model is used to analyze the natural frequency and seismic response of cylinders.

Keywords: Water-cylinder interaction, Surface wave, Water compressibility, Seabed flexibility, Added mass, Wave and earthquake action

1 Introduction

With the development of the economy and transportation, more and more offshore and coastal structures, such as bridge piers and offshore wind turbines, have been constructed in China in recent years. These structures may be under threat of earthquakes in areas of active seismicity, for instance, the Eastern coast of China. It is well known that water-structure interaction causes hydrodynamic pressure on the structure during earthquakes and the additional hydrodynamic pressure has significant effect on the dynamic responses and properties of the structure (Liaw and Chopra 1974; Han and Xu 1996; Wei et al. 2013). Therefore, it is necessary to investigate earthquake-induced hydrodynamic pressure on the offshore structures. The purpose of this study is mainly to develop an accurate frequency-domain model of water interaction with cylinders of arbitrary shape during earthquakes.

The study on earthquake-induced hydrodynamic pressure has begun with the gravity dams (Westergaard 1933) and the cantilever circular cylinders (Jacobsen 1949). For the simple cross-section cylinder, it has been well studied by analytical method, such as circular cylinder (Liaw and Chopra 1974; Tanaka and Hudspeth 1988), elliptical cylinder (Wang et al. 2018a, 2019a), and arbitrary smooth cross-section (Wang et al. 2018b). Liaw and Chopra (1974) demonstrated that water compressibility was negligible for slender cylinders but important for squat cylinders vibrating at high frequency. Additionally, effect of the hydrodynamic pressure can be simply modeled as an 'added mass' when the surface wave and water compressibility are ignored. Assuming the structure rigid, the simplified formulas of the added mass for the earthquake induced hydrodynamic pressure on circular cylinder and elliptical cylinders were given by Jiang et al. (2017), Li and Yang (2013), and Wang et al. (2018a). Considering the flexible of the structure, a simple and accurate added mass representation was also presented by Han and Xu (1996). Later, Wang et al. extended this model to calculate the added mass representation for a flexible vertical elliptical cylinder vibrating in water (Wang et al. 2019a). Considering water compressibility, Du et al. (2014) presented a simplified formula in time domain for hydrodynamic pressure on rigid circular cylinders by introducing three dimensionless parameters including frequency ratio, wide-depth ratio and relative height. Recently, considering the flexible of the circular cylinder, an accurate and efficient time-domain model was proposed to analyze water-cylinder interaction during earthquake (Wang et al. 2018c). In addition, the boundary integral method is also can be used to analyze the earthquake responses of submerged circular cylinder (Williams 1986).

The earthquake-induced hydrodynamic pressure on complex structures should be solved by numerical method, such as the finite element method (FEM) (Liao 1986, Liaw and Chopra 1974), finite-difference scheme (Chen 1997), and the finite element technique incorporating the infinite element (Woo-Sun et al. 1991). A special boundary method based on the use of a complete and non-singular set of Trefftz functions was presented for hydrodynamic pressure on axisymmetric offshore structures (Sun and Nogami 2010; Avilés and Li 2001). The free surface wave effect on the water-cylinder interaction is significant in wave force (Ti et al. 2020), but it has been validated that free surface waves have less effect on the earthquake-induced hydrodynamic force on cylinders by Liaw and Chopra (1974) and Li and Yang (2013).

Recently, coupled the FEM and artificial boundary condition was used to simulated the water-fluid interaction system (Zhao et al. 2018). Wang et al. (2019b) present an accurate and efficient numerical model to calculate the earthquake-induced hydrodynamic pressure on uniform vertical cylinders with an arbitrary cross section surrounded by water and the simplified formulas for the hydrodynamic pressure on round-ended and rectangular cylinder were also given. In addition, the simplified methods for efficient seismic design and analysis of water-surrounded circular tapered cylinders and composite axisymmetric structures were also presented (Wang et al. 2018d, 2019c).

Recently, the scaled boundary finite element method (SBFEM), originally developed to solve soil-structure interaction problems (Song and Wolf 1996, 1997), has been successfully applied to many fields, such as stress singularities as occurring in cracks (Song and Wolf 2002), elastostatics (Deeks and Wolf 2002), potential flow (Deeks and

Cheng 2003), and non-linear analysis of unbounded media (Doherty and Deeks 2005). The SBFEM is a novel semi-analytical, combining the advantages of the finite element method (FEM) and the boundary element method (BEM), as reduction of the spatial dimension by one but no fundamental solution required and eliminates singular integrals. The SBFEM is also used to analyze wave interaction with a bottom-mounted uniform porous cylinder of arbitrary shape (Meng and Zou 2012), a single and multiple cylindrical structures of different cross sectional shape (Song et al. 2010).

In this paper, a substructure method in frequency domain is proposed for the analysis of seismic response of the water-cylinder interaction system, where the section of cylinder can be general shape. Proposed approach is efficient in the water-cylinder dynamic interaction. The SBFEM is used to simulate the earthquake-induced hydrodynamic pressure on the uniform vertical cylinder with arbitrary cross section. Firstly, utilizing the variables separation method, the three-dimensional wave equation governing the compressible water is transformed into a two-dimensional (2D) Helmholtz equation. Secondly, a dynamic-stiffness equation is obtained by utilizing the SBFEM. Thirdly, a continued fraction is used to solve the dynamic-stiffness equation. Finally, the finite element equation of the water-cylinder interaction system is obtained.

2 Mathematical formulation

The water-cylinder interaction system during earthquake is shown in Fig. 1. The structure can be assumed to be linearly elastic. The cylinder varies uniformly from bedrock above water surface along z axis. The water is a horizontally infinite layer of the constant depth h. The rigid bedrock has a horizontal earthquake motion of the displacement time history along the direction of paralleling x axis. The cylinder is fully submerged in water and treated simply as a one-dimensional structure governed by beam theory. The water-cylinder interaction system is initially at rest.

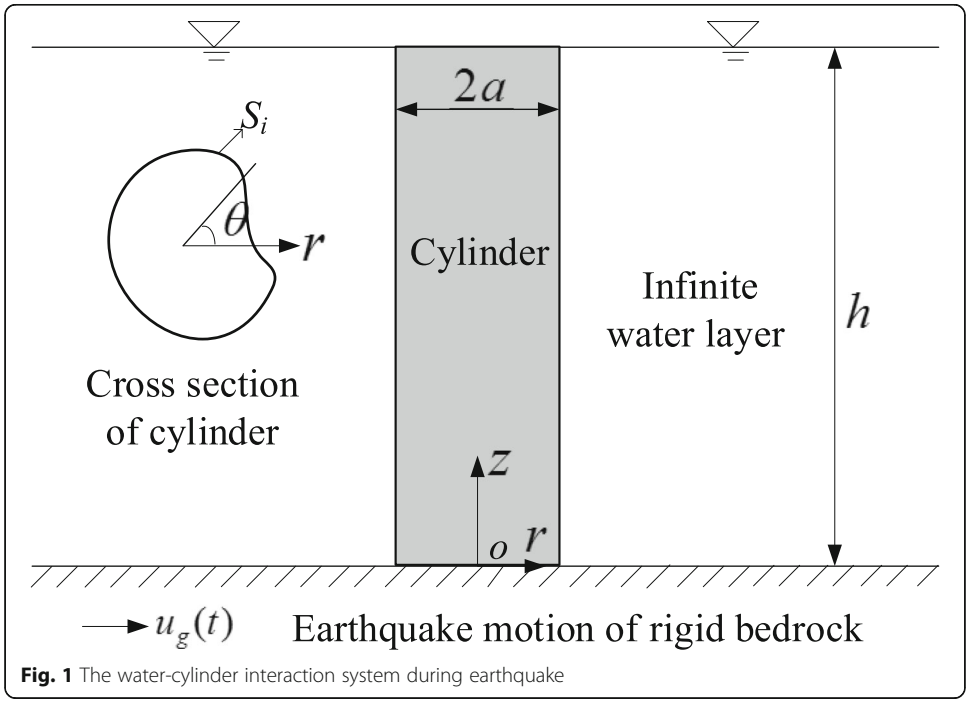

Fig. 1 The water-cylinder interaction system during earthquake

The governing equation of the water can be expressed in terms of its hydrodynamic pressure, which is controlled by the wave equation, can be written as

$$\frac{\partial^2 P}{\partial x^2}+\frac{\partial^2 P}{\partial y^2}+\frac{\partial^2 P}{\partial z^2}+\frac{\omega^2}{c^2}P=0 \tag{1}$$

where $P(x, y, z, \omega)$ is the hydrodynamic pressure expressed in frequency domain; ω is the circle frequency; $c = 1438$m/s is the velocity of the wave propagate in water.

The boundary conditions are as follows

(1) At the bottom of the water, no vertical motion

$$\frac{\partial P}{\partial z}=0 \tag{2a}$$

(2) At the free surface of the water, the hydrodynamic pressure is zero

$$P=0 \tag{2b}$$

(3) At the water-cylinder interface, the outward normal acceleration of the water in contact with the structure is equal the cylinder surface, which in frequency can be written as

$$\frac{\partial P}{\partial n}=\rho_w \omega^2 U_x n_x \tag{2c}$$

(4) At the infinity of the water, the hydrodynamic pressure is decayed to zero

$$P|_{r=\infty}=0 \tag{2d}$$

where n_x is the outward normal direction of the cylinder surface at the x axis component; U_x is the displacement of the cylinder surface in x-direction; $\rho_w = 1000$ kg/m^3 is the mass density of water; and r is the distance from the cylinder.

Applying separation of the variables to the hydrodynamic pressure, the vertical modes of the hydrodynamic pressure are obtained. Then, the hydrodynamic pressure $P(x, y, z, \omega)$ can be separated out as (Liaw and Chopra 1974)

$$P(x, y, z, \omega) = \sum_{j=1}^{\infty} P_j U_j \cos\lambda_j z \tag{3}$$

where $P_j = P_j(x, y, \omega)$ is the modal hydrodynamic pressure in xy-plane; $\lambda_j = (2j - 1)\pi/2h$; and $U_j = \frac{2}{h}\int_0^h U_x n_x \cos\lambda_j z dz$ is the corresponding modal displacement of the cylinder.

Then, the problem of three-dimensional water-cylinder interaction is reduced to solve a two-dimensional Helmholtz equation with the boundary conditions (Liaw and Chopra 1974) as follows

$$\frac{\partial^2 P_j}{\partial x^2} + \frac{\partial^2 P_j}{\partial y^2} + \left(\frac{\omega^2}{c^2} - \lambda_j^2\right) P_j = 0 \tag{4}$$

$$\frac{\partial P_j}{\partial n} = \omega^2 \rho_w n_x \tag{5a}$$

$$P_j|_{r=\infty} = 0 \tag{5b}$$

3 The SBFEM equation

3.1 Scaled boundary finite element transformation

SBFEM defines the domain V by scaling a defining curve S_i relative to a scaling center $(x_0\ y_0)$, which is chosen at the center of the cylinder in this study. As shown in Fig. 2, the circumferential coordinate η is anticlockwise along the defining curve S_i, which is closed in this case. The normalized radial coordinate ξ is a scaling factor with $1 \le \xi \le \infty$ for unbounded domain. The coordinate of a point on the straight line element are denote as x_b and y_b, it can be expressed with mapping function as

$$x_b = \mathbf{NX} \tag{6a}$$

$$y_b = \mathbf{NY} \tag{6b}$$

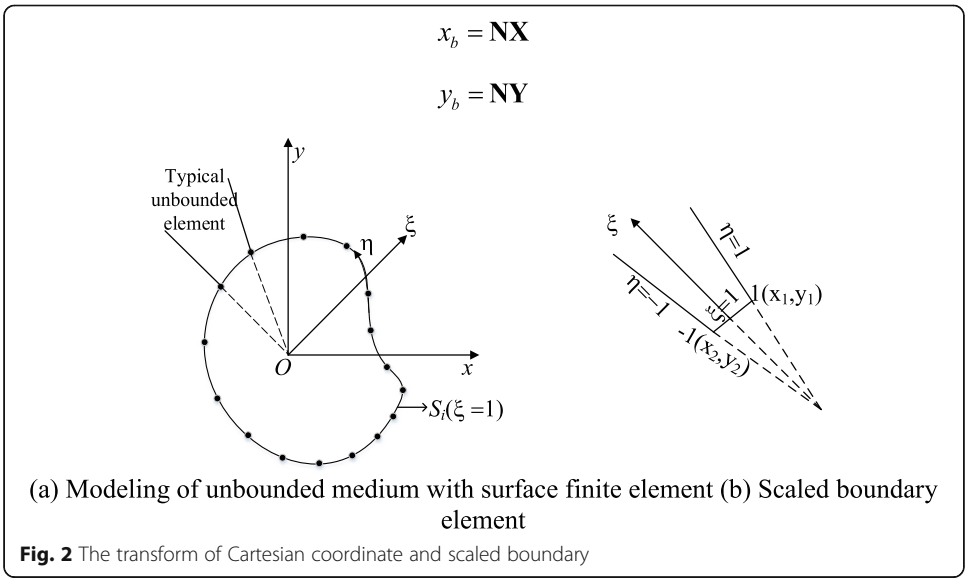

(a) Modeling of unbounded medium with surface finite element (b) Scaled boundary element

Fig. 2 The transform of Cartesian coordinate and scaled boundary

with $\mathbf{N}=\left[\frac{1-\eta}{2} \quad \frac{1+\eta}{2}\right]$ is the mapping function; $\mathbf{X}=\{x_1 \quad x_2\}^T$, $\mathbf{Y}=\{y_1 \quad y_2\}^T$ are the nodes coordinates vector in Cartesian coordinate.

Therefore, the Cartesian coordinates are transformed to the scaled boundary coordinate ξ and η with the scaling equations

$$x = \xi x_b \tag{7a}$$

$$y = \xi y_b \tag{7b}$$

The spatial derivatives in the two coordinate systems are related as

$$\begin{Bmatrix} \frac{\partial}{\partial \xi} \\ \frac{\partial}{\partial \eta} \end{Bmatrix} = \hat{\mathbf{J}}(\xi,\eta) \begin{Bmatrix} \frac{\partial}{\partial x} \\ \frac{\partial}{\partial y} \end{Bmatrix} \tag{8}$$

with

$$\hat{\mathbf{J}}(\xi,\eta) = \begin{bmatrix} x_b & y_b \\ \xi x_b,\eta & \xi y_b,\eta \end{bmatrix} = \begin{bmatrix} 1 & \\ & \xi \end{bmatrix} \mathbf{J} \tag{9}$$

where $\mathbf{J} = \begin{bmatrix} x_b & y_b \\ x_b,\eta & y_b,\eta \end{bmatrix}$ is Jacobi matrix.

Then the derivatives with respect to x, y can be obtained

$$\begin{Bmatrix} \frac{\partial}{\partial x} \\ \frac{\partial}{\partial y} \end{Bmatrix} = \hat{\mathbf{J}}(\xi,\eta)^{-1} \begin{Bmatrix} \frac{\partial}{\partial \xi} \\ \frac{\partial}{\partial \eta} \end{Bmatrix} = \mathbf{b}_1 \frac{\partial}{\partial \xi} + \frac{1}{\xi}\mathbf{b}_2 \frac{\partial}{\partial \eta} \tag{10}$$

with

$$\mathbf{b}_1 = \frac{1}{|\mathbf{J}|} \begin{Bmatrix} y_{b,\eta} \\ -x_{b,\eta} \end{Bmatrix} \tag{11a}$$

$$\mathbf{b}_2 = \frac{1}{|\mathbf{J}|} \begin{Bmatrix} -y_b \\ x_b \end{Bmatrix} \tag{11b}$$

For later use, note that $(\mathbf{b}_2|\mathbf{J}|)_{,\eta} = -\mathbf{b}_1|\mathbf{J}|$.

The infinitesimal area $\mathrm{d}V$ of the domain is calculated as

$$\mathrm{d}V = \left|\hat{\mathbf{J}}(\xi,\eta)\right|\mathrm{d}\xi\mathrm{d}\eta = \xi|\mathbf{J}|\mathrm{d}\xi\mathrm{d}\eta \tag{12a}$$

$$\mathrm{d}S = \sqrt{x_{,\eta}{}^2 + y_{,\eta}{}^2}\mathrm{d}\eta \tag{12b}$$

3.2 Scaled boundary finite element equation

To derive the finite element approximation, Eq. (4) is multiplied by a weighting function w and integrating over the domain, it can be obtained as

$$\int w\left(\frac{\partial^2 P_j}{\partial x^2} + \frac{\partial^2 P_j}{\partial y^2} + \left(\frac{\omega^2}{c^2} - \lambda^2\right)P_j\right)\mathrm{d}V = 0 \tag{13}$$

Substituting Eq. (10) into Eq. (13), we get

$$\int \left(w\mathbf{b}_1{}^T \frac{\partial}{\partial \xi} \left(\mathbf{b}_1 \frac{\partial P_j}{\partial \xi} + \mathbf{b}_2 \frac{\partial P_j}{\partial \eta} \right) + \frac{1}{\xi} w\mathbf{b}_2{}^T \frac{\partial}{\partial \eta} \left(\mathbf{b}_1 \frac{\partial P_j}{\partial \xi} + \mathbf{b}_2 \frac{\partial P_j}{\partial \eta} \right) + w \left(\frac{\omega^2}{c^2} - \lambda^2 \right) P_j \right) \mathrm{d}V = 0 \quad (14)$$

Substituting the transformation of the scaled boundary coordinate into Eq. (14), the SBFEM equation can be obtained as

$$\mathbf{E}_0 \xi^2 \mathbf{P}_{j,\xi\xi} + \left(\mathbf{E}_0 - \mathbf{E}_1 + \mathbf{E}_1{}^T \right) \xi \mathbf{P}_{j,\xi} - \mathbf{E}_2 \mathbf{P}_j + \left(\frac{\omega^2}{c^2} - \lambda^2 \right) \mathbf{M}_0 \xi^2 \mathbf{P}_j = \mathbf{0} \quad (15)$$

with the introducing coefficient matrixes are

$$\mathbf{E}_0 = \int_{-1}^{1} \mathbf{B}_1{}^T \mathbf{B}_1 |\mathbf{J}| d\eta = \frac{\Delta_x{}^2 + \Delta_y{}^2}{12|\mathbf{J}|} \begin{bmatrix} 2 & 1 \\ 1 & 2 \end{bmatrix} \quad (16a)$$

$$\mathbf{E}_1 = \int_{-1}^{1} \mathbf{B}_2{}^T \mathbf{B}_1 |\mathbf{J}| d\eta = \frac{\Delta_x{}^2 + \Delta_y{}^2}{24|\mathbf{J}|} \begin{bmatrix} -1 & 1 \\ 1 & -1 \end{bmatrix} - \frac{\Delta_y(y_1 + y_2) + \Delta_x(x_1 + x_2)}{8|\mathbf{J}|} \begin{bmatrix} -1 & -1 \\ 1 & 1 \end{bmatrix} \quad (16b)$$

$$\mathbf{E}_2 = \int_{-1}^{1} \mathbf{B}_2{}^T \mathbf{B}_2 |\mathbf{J}| d\eta = \frac{3(y_1 + y_2)^2 + 3(x_1 + x_2)^2 + \Delta_x{}^2 + \Delta_y{}^2}{24|\mathbf{J}|} \begin{bmatrix} 1 & -1 \\ -1 & 1 \end{bmatrix} \quad (16c)$$

$$\mathbf{M}_0 = \int_{-1}^{1} \mathbf{N}^T \mathbf{N} |\mathbf{J}| d\eta = \frac{|\mathbf{J}|}{3} \begin{bmatrix} 2 & 1 \\ 1 & 2 \end{bmatrix} \quad (16d)$$

where $\mathbf{B}_1 = \mathbf{b}_1 \mathbf{N}$ and $\mathbf{B}_2 = \mathbf{b}_2 \mathbf{N}_{,\eta}$.

To simply the nomenclature, the same symbols are used for the assembled coefficient matrices.

3.3 Dynamic-stiffness equation

The amplitude of the internal nodal forces $\mathbf{Q}(\xi)$, which are equal to the normal derivatives of P_j, on a line with a constant ξ are addressed. Applying the principle of virtual work yields

$$\mathbf{w}^T \mathbf{Q}(\xi) = \int_{S_i} \mathbf{w}^T \frac{\partial P_j}{\partial n} \mathrm{d}S \quad (17)$$

The nodal forces can be obtained by substituting relevant formulas mentioned above

$$\mathbf{Q}(\xi) = \mathbf{E}_0 \xi \mathbf{P}_{j,\xi} + \mathbf{E}_1{}^T \mathbf{P}_j \quad (18)$$

For an unbounded medium, the amplitudes of the modal nodal forces $\mathbf{R}(\xi)$ are equal to the opposite of the internal nodal forces $\mathbf{Q}(\xi)$, which can be expressed as

$$\mathbf{R}(\xi) = -\mathbf{Q}(\xi) \quad (19)$$

The same signs of Eqs. (18) and (19) applied to the assembled system. In the frequency domain, the amplitudes of the modal hydrodynamic pressures $\mathbf{P}_j(\xi)$ are related to those of the nodal forces $\mathbf{R}(\xi)$ as

$$\mathbf{R}(\xi) = \mathbf{S}(\omega, \xi) \mathbf{P}_j(\xi) \quad (20)$$

where $\mathbf{S}(\omega, \xi)$ is the dynamic-stiffness matrix.

The SBFE equation in dynamic-stiffness is derived from Eqs. (15), (18), (19) and (20) (Song and Wolf 1996). On the boundary ($\xi = 1$) the dynamic stiffness matrix for the unbounded medium is expressed as

$$(\mathbf{S}(\omega)+\mathbf{E}_1)\mathbf{E}_0{}^{-1}\left(\mathbf{S}(\omega)+\mathbf{E}_1{}^{T}\right)-\omega\mathbf{S}(\omega)_{,\omega}-\mathbf{E}_2+\left(\frac{\omega^2}{c^2}-\lambda^2\right)\mathbf{M}_0=\mathbf{0} \tag{21}$$

Introducing a dimensionless coefficient $\varpi=-i\lambda\sqrt{1-(\omega/\lambda c)^2}$, Eq. (21) can be simplified into the general form of the SBFEM as (Song and Wolf 1996)

$$(\mathbf{S}(\varpi)+\mathbf{E}_1)\mathbf{E}_0{}^{-1}\left(\mathbf{S}(\varpi)+\mathbf{E}_1{}^{T}\right)-\varpi\mathbf{S}(\varpi)_{,\mathrm{a}}-\mathbf{E}_2+\varpi^2\mathbf{M}_0=\mathbf{0} \tag{22}$$

3.4 Solution of the dynamic-stiffness

It can be seen that Eq. (22) is a system of non-linear first-order ordinary differential equations with the independent variable ϖ. To avoid the computationally expensive task, a continued fraction solution for the dynamic-stiffness matrix is developed in (Bazyar and Song 2008) directly from the scaled boundary finite element equation.

The continued fraction solution of the dynamic-stiffness matrix is derived in this section. The solution is assumed as

$$\mathbf{S}(\varpi)=\mathbf{g}_0+i\varpi\mathbf{h}_0-\mathbf{S}_1{}^{-1}(\varpi) \tag{23a}$$

$$\mathbf{S}_j{}^{-1}(\varpi)=\mathbf{g}_j+i\varpi\mathbf{h}_j-\mathbf{S}_{j+1}{}^{-1}(\varpi) \tag{23b}$$

Substituting Eq. (23a) into (22), three terms in descending order of the power of $(i\varpi)$ are expressed as

$$\begin{aligned}&(i\varpi)^2\left(\mathbf{h}_0\mathbf{E}_0^{-1}\mathbf{h}_0-\mathbf{M}_0{}'\right)+(i\varpi)\left[\mathbf{h}_0\mathbf{E}_0{}^{-1}\left(\mathbf{g}_0+\mathbf{E}_1^{T}\right)+(\mathbf{g}_0+\mathbf{E}_1)\mathbf{E}_0^{-1}\mathbf{h}_0-\mathbf{h}_0\right]\\&+(\mathbf{g}_0+\mathbf{E}_1)\mathbf{E}_0^{-1}\left(\mathbf{g}_0+\mathbf{E}_1^{T}\right)+\mathbf{E}_2-(\mathbf{g}_0+\mathbf{E}_1)\mathbf{E}_0^{-1}\mathbf{S}_1^{-1}-(i\varpi)\mathbf{h}_0\mathbf{E}_0^{-1}\mathbf{S}_1^{-1}\\&-\mathbf{S}_1{}^{-1}\mathbf{E}_0{}^{-1}\left(\mathbf{g}_0+\mathbf{E}_1^{T}\right)-\mathbf{S}_1^{-1}\mathbf{E}_0^{-1}(i\varpi)\mathbf{h}_0+\mathbf{S}_1^{-1}\mathbf{E}_0^{-1}\mathbf{S}_1^{-1}-\varpi\mathbf{S}_{1,\varpi}^{-1}=\mathbf{0}\end{aligned} \tag{24}$$

It can be seen that Eq. (24) is satisfied only when all the three terms are equal to zero, setting the coefficient of the $(i\varpi)^2$ and $(i\varpi)$ terms to zero results in

$$\mathbf{h}_0\mathbf{E}_0^{-1}\mathbf{h}_0-\mathbf{M}_0{}'=\mathbf{0} \tag{25a}$$

$$\mathbf{h}_0\mathbf{E}_0{}^{-1}\left(\mathbf{g}_0+\mathbf{E}_1^{T}\right)+(\mathbf{g}_0+\mathbf{E}_1)\mathbf{E}_0^{-1}\mathbf{h}_0-\mathbf{h}_0=\mathbf{0} \tag{25b}$$

where Eq. (25a) can be solved by the function 'care' in MATLAB, and Eq. (25b) can be solved by the function 'lyap' in MATLAB.

The remaining part of Eq. (24) which is an equation for $\mathbf{S}_1$ can be written as

$$\mathbf{S}_1\mathbf{V}_1{}^{1}\mathbf{S}_1+\left(\mathbf{V}_2{}^{1}+i\varpi\mathbf{V}_3{}^{1}\right)\mathbf{S}_1+\mathbf{S}_1\left(\mathbf{V}_4{}^{1}+i\varpi\mathbf{V}_5{}^{1}\right)+\mathbf{V}_6^{1}-\varpi\mathbf{S}_{1,\varpi}=\mathbf{0} \tag{26}$$

with

$$\mathbf{V}_1{}^{1}=(\mathbf{g}_0+\mathbf{E}_1)\mathbf{E}_0^{-1}\left(\mathbf{g}_0+\mathbf{E}_1^{T}\right)+\mathbf{E}_2 \tag{27a}$$

$$\mathbf{V}_2{}^{1}=-\mathbf{E}_0{}^{-1}\left(\mathbf{g}_0+\mathbf{E}_1^{T}\right) \tag{27b}$$

$$\mathbf{V}_3{}^{1}=-\mathbf{E}_0{}^{-1}\mathbf{h}_0 \tag{27c}$$

$$\mathbf{V}_4{}^{1}=-(\mathbf{g}_0+\mathbf{E}_1)\mathbf{E}_0^{-1} \tag{27d}$$

$$\mathbf{V}_5{}^{1}=-\mathbf{h}_0\mathbf{E}_0^{-1} \tag{27e}$$

$$\mathbf{V}_6{}^1 = \mathbf{E}_0{}^{-1} \tag{27f}$$

Substituting Eq. (23b) into Eq. (26), three terms in descending order of the power of $(i\varpi)$ are expressed as

$$\begin{aligned}&(i\varpi)^2\left(\mathbf{h}_j\mathbf{V}_1{}^j\mathbf{h}_j+\mathbf{V}_3{}^j\mathbf{h}_j+\mathbf{h}_j\mathbf{V}_5{}^j\right)+(i\varpi)\left(\mathbf{h}_j\mathbf{V}_1{}^j\mathbf{g}_j+\mathbf{g}_j\mathbf{V}_1{}^j\mathbf{h}_j+\mathbf{V}_2{}^j\mathbf{h}_j+\mathbf{V}_3{}^j\mathbf{g}_j+\mathbf{h}_j\mathbf{V}_4{}^j+\mathbf{g}_j\mathbf{V}_5{}^j-\mathbf{h}_j\right)\\&+\mathbf{g}_j\mathbf{V}_1{}^j\mathbf{g}+\mathbf{V}_6^j+\mathbf{V}_2{}^j\mathbf{g}_j+\mathbf{g}_j\mathbf{V}_4{}^j-\mathbf{S}_{j+1}{}^{-1}\left[\mathbf{V}_1{}^j\left(\mathbf{g}_j+ia\mathbf{h}_j\right)+\mathbf{V}_4{}^j+ia\mathbf{V}_5{}^j\right]\\&-\left[\left(\mathbf{g}_j+ia\mathbf{h}_j\right)\mathbf{V}_1{}^j+\mathbf{V}_2{}^j+ia\mathbf{V}_3{}^j\right]\mathbf{S}_{j+1}{}^{-1}+\mathbf{S}_{j+1}{}^{-1}\mathbf{V}_1{}^j\mathbf{S}_{j+1}{}^{-1}+\varpi\mathbf{S}_{j+1,\varpi}{}^{-1}=0\end{aligned} \tag{28}$$

Equation (28) is satisfied when all the three terms are equal to zero, setting the coefficient of the $(i\varpi)^2$ and $(i\varpi)$ terms to zero results in

$$\mathbf{h}_j\mathbf{V}_1{}^j\mathbf{h}_j+\mathbf{V}_3{}^j\mathbf{h}_j+\mathbf{h}_j\mathbf{V}_5{}^j=\mathbf{0} \tag{29a}$$

$$\mathbf{h}_j\mathbf{V}_1{}^j\mathbf{g}_j+\mathbf{g}_j\mathbf{V}_1{}^j\mathbf{h}_j+\mathbf{V}_2{}^j\mathbf{h}_j+\mathbf{V}_3{}^j\mathbf{g}_j+\mathbf{h}_j\mathbf{V}_4{}^j+\mathbf{g}_j\mathbf{V}_5{}^j-\mathbf{h}_j=\mathbf{0} \tag{29b}$$

Pre- and post-multiplying Eq. (29a) with $\mathbf{h}_j^{-1}$ respectively yields

$$\mathbf{V}_1{}^j+\mathbf{h}_j^{-1}\mathbf{V}_3{}^j+\mathbf{V}_5{}^j\mathbf{h}_j^{-1}=\mathbf{0} \tag{30}$$

Equations (29b) and (30) can be solved by the function 'layp' in MATLAB. Then the remaining part of Eq. (28) is an equation for $\mathbf{S}_{j+1}$ (Bazyar and Song 2008)

$$\mathbf{S}_{j+1}\mathbf{V}_1{}^{j+1}\mathbf{S}_{j+1}+\left(\mathbf{V}_2{}^{j+1}+i\varpi\mathbf{V}_3{}^{j+1}\right)\mathbf{S}_{j+1}+\mathbf{S}_{j+1}\left(\mathbf{V}_4{}^{j+1}+i\varpi\mathbf{V}_5{}^{j+1}\right)+\mathbf{V}_6^{j+1}-\varpi\mathbf{S}_{j+1,\varpi}=\mathbf{0} \tag{31}$$

with

$$\mathbf{V}_1{}^{j+1}=\mathbf{g}_j\mathbf{V}_1{}^j\mathbf{g}+\mathbf{V}_6^j+\mathbf{V}_2{}^j\mathbf{g}_j+\mathbf{g}_j\mathbf{V}_4{}^j \tag{32a}$$

$$\mathbf{V}_2{}^{j+1}=-\left(\mathbf{V}_1{}^j\mathbf{g}_j+\mathbf{V}_4{}^j\right) \tag{32b}$$

$$\mathbf{V}_3{}^{j+1}=-\left(\mathbf{V}_1{}^j\mathbf{h}_j+\mathbf{V}_5{}^j\right) \tag{32c}$$

$$\mathbf{V}_4{}^{j+1}=-\left(\mathbf{g}_j\mathbf{V}_1{}^j+\mathbf{V}_2{}^j\right) \tag{32d}$$

$$\mathbf{V}_5{}^{j+1}=-\left(\mathbf{h}_j\mathbf{V}_1{}^j+\mathbf{V}_3{}^j\right) \tag{32e}$$

$$\mathbf{V}_6{}^{j+1}=\mathbf{V}_1{}^j \tag{32f}$$

The continued fraction solution of Eq. (23) is constructed from the coefficient matrix $\mathbf{g}_0$, $\mathbf{h}_0$, $\mathbf{g}_j$, $\mathbf{h}_j$, and $\mathbf{S}_j^{-1}$, which can be solved by Eqs. (27), (29b) and (30).

3.5 Scaled boundary finite element transformation

The same weight residual method used to the boundary condition Eq. (5a), and transformed to the scaled boundary coordinates, it can be obtained that

$$\mathbf{E}_0\xi\mathbf{P}_{j,\xi}+\mathbf{E}_1{}^T\mathbf{P}_j=-\omega^2\mathbf{M}_1\mathbf{n}_x \tag{33}$$

with

$$\mathbf{n}_x=\begin{pmatrix}n_{x1} & n_{x2}\end{pmatrix}^{\mathrm{T}} \tag{34a}$$

$$\mathbf{M}_1 = \rho_w \int_{-1}^{1} \overline{\mathbf{N}}^T \mathbf{N} d\eta \tag{34b}$$

where $\overline{\mathbf{N}}$ is the mapping function of the structure, and $\mathbf{M}_1$ is lumped as

$$\mathbf{M}_1 = \frac{\rho_w l_e}{2} \begin{bmatrix} 1 & 0 \\ 0 & 1 \end{bmatrix} \tag{35}$$

It is obvious that the left of Eq. (33) is the internal nodal force $\mathbf{Q}(\xi)$. The same signs in Eq. (33) applied to the assembled system. Substituting Eqs. (19) and (20) into Eq. (33), the relation of the hydrodynamic pressure and the displacement of the cylinder at the interface can be obtained as

$$\mathbf{P}_j = \omega^2 [\mathbf{S}(\varpi)]^{-1} \mathbf{M}_1 \mathbf{n} \tag{36}$$

4 Coupled finite element equation of water-cylinder interaction system

The cylinder is assumed as a cantilever only the lateral deformation is considered, which can be solved by the finite element method (Chandrupatla and Belegundu 2013). After the spatial discretization to the cylinder, the finite element equation can be written as the partitioned matrix form as follow

$$\begin{bmatrix} \mathbf{M}_O & \boldsymbol{0} \\ \boldsymbol{0} & \mathbf{M}_I \end{bmatrix} \begin{Bmatrix} \ddot{\mathbf{u}}_O \\ \ddot{\mathbf{u}}_I \end{Bmatrix} + \begin{bmatrix} \mathbf{C}_O & \mathbf{C}_{OI} \\ \mathbf{C}_{IO} & \mathbf{C}_I \end{bmatrix} \begin{Bmatrix} \dot{\mathbf{u}}_O \\ \dot{\mathbf{u}}_I \end{Bmatrix} + \begin{bmatrix} \mathbf{K}_O & \mathbf{K}_{OI} \\ \mathbf{K}_{IO} & \mathbf{K}_I \end{bmatrix} \begin{Bmatrix} \mathbf{u}_O \\ \mathbf{u}_I \end{Bmatrix} = \begin{Bmatrix} \boldsymbol{0} \\ \mathbf{f}_I \end{Bmatrix} \tag{37}$$

where the subscripts I denotes the nodes of the cylinder immersed in water and O denotes the nodes of the cylinder in air, respectively; u is the absolute motion vector with the given bedrock motion u_g; the dot over variable represents the derivative to time; and M, C and K are the lumped mass, damping and stiffness matrices, respectively, and $\mathbf{f}_I$ is the hydrodynamic force vector caused by the water-cylinder interaction. The element stiffness matrix is obtained as Re. (Chandrupatla and Belegundu 2013).

By using Fourier transform, Eq. (37) can be rewritten as

$$-\omega^2 \begin{bmatrix} \mathbf{M}_O & 0 \\ 0 & \mathbf{M}_I \end{bmatrix} \begin{Bmatrix} \mathbf{U}_O \\ \mathbf{U}_I \end{Bmatrix} + (i\omega) \begin{bmatrix} \mathbf{C}_O & \mathbf{C}_{OI} \\ \mathbf{C}_{IO} & \mathbf{C}_I \end{bmatrix} \begin{Bmatrix} \mathbf{U}_O \\ \mathbf{U}_I \end{Bmatrix} + \begin{bmatrix} \mathbf{K}_O & \mathbf{K}_{OI} \\ \mathbf{K}_{IO} & \mathbf{K}_I \end{bmatrix} \begin{Bmatrix} \mathbf{U}_O \\ \mathbf{U}_I \end{Bmatrix} = \begin{Bmatrix} 0 \\ \mathbf{F}_I \end{Bmatrix} \tag{38}$$

The cantilever immersed in water is separated into N nodes, the corresponding z-coordinates, lateral deformations and mapping functions are

$$\mathbf{z}_I = \{ z_1 \quad z_2 \quad \cdots \quad z_N \}^T \tag{39a}$$

$$\mathbf{U}_I = \{ U_{I1} \quad U_{I2} \quad \cdots \quad U_{IN} \}^T \tag{39b}$$

$$\mathbf{N}_Z(z) = \{ N_1(z) \quad N_2(z) \quad \cdots \quad N_N(z) \} \tag{39c}$$

Then arbitrary node coordinate and deformation can be expressed as

$$z = \mathbf{N}_z(z) \mathbf{z}_I \tag{40a}$$

$$U = \mathbf{N}_z \mathbf{U}_I \tag{40b}$$

The shape function is defined as

$$\mathbf{W} = \int_0^h [\mathbf{N}_z(z)]^{\mathrm{T}} \mathbf{N}_z(z) \mathrm{d}z \tag{41}$$

The corresponding modal vector is written as

$$\boldsymbol{\phi}_j = \left\{ \cos(\lambda_j z_1) \quad \cos(\lambda_j z_2) \quad \cdots \quad \cos(\lambda_j z_{\mathrm{N}}) \right\}^{\mathrm{T}} \tag{42}$$

Substituting Eq. (41) into the modal displacement, we get

$$U_j = \frac{2}{h} \left[\boldsymbol{\phi}_j\right]^{\mathrm{T}} \mathbf{W} \mathbf{U}_{\mathrm{I}} \tag{43}$$

The interaction force in Eq. (38) is

$$\mathbf{F}_{\mathrm{I}} = \int_0^h \mathbf{N}^{\mathrm{T}} F \mathrm{d}z \tag{44}$$

with the continuous hydrodynamic force equal to the integral along interface S_i

$$F = \sum_{j=1}^{\infty} - \int_S \mathbf{P}_j . \mathbf{n}_x \mathrm{d}s U_j \cos\lambda_j z = \sum_{j=1}^{\infty} f_j U_j \cos\lambda_j z \tag{45}$$

where $f_j = - \int_S \mathbf{P}_j . \mathbf{n}_x \mathrm{d}s$, where the dot between two vector is the inner product of the vectors.

Substituting Eqs. (43) and (45) into Eq. (44), the hydrodynamic force can be expressed as follows

$$\mathbf{F}_{\mathrm{I}} = - \tilde{\mathbf{S}} \mathbf{U}_{\mathrm{I}} \tag{46}$$

$$\tilde{\mathbf{S}} = \frac{2}{h} \sum_{j=1}^{\infty} f_j \mathbf{W} \boldsymbol{\phi}_j \boldsymbol{\phi}_j^{\mathrm{T}} \mathbf{W} \tag{47}$$

5 Verification and application

The definition of section parameters is shown in Fig. 3. Then, the seismic responses of circular, elliptical and rectangle cylinders are investigated, where the density, Yang's modulus and damping ratio of the cylinder is 2500 kg/m3, 30,000 MPa and 0.05.

5.1 Verification

The accuracy of the present method is verified by comparing the hydrodynamic force on rigid circular, elliptical and rectangle cylinders with the analytical or numerical

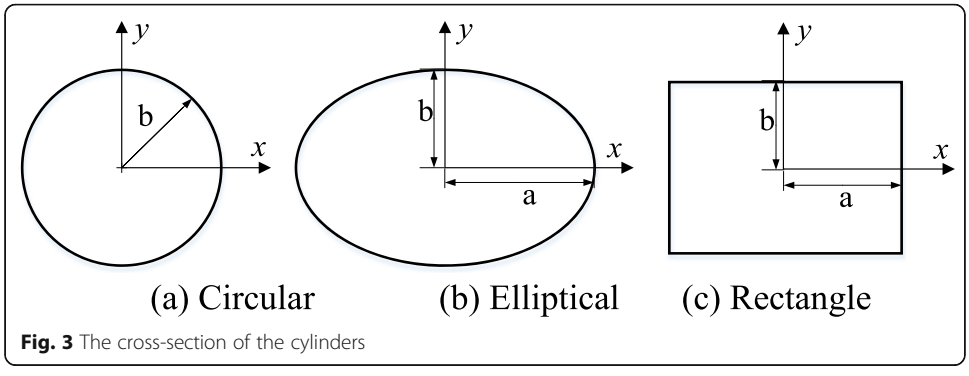

Fig. 3 The cross-section of the cylinders

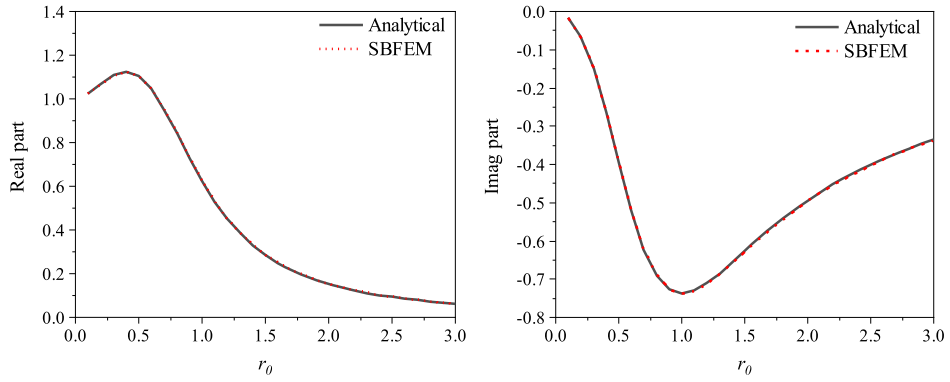

Fig. 4 The hydrodynamic pressure on the rigid circular model in frequency

solutions (Wang et al. 2018a, 2019a; Du et al. 2014), where the numerical solution is calculated by finite element method.

Figure 4 shows the real and the imaginary part of the hydrodynamic force on circular cylinder, where the horizontal axis is $r_0 = \varpi$, 'SBFEM', and 'Analytical' represent the solution calculated by the proposed method and the analytical solution. Figures 5 and 6 shows the real and the imaginary part of the hydrodynamic force on elliptical and rectangle cylinders, where 'Numerical' represents the numerical solution. It can be seen that the proposed method is in good agreement with the reference solution.

5.2 Application

The seismic responses and natural frequencies of circular, elliptical and rectangle cylinders are further investigated. The seismic responses of cylinders surrounded by water in frequency domain are analyzed by using ground excitation $u_g = e^{i\omega t}$. Two dimensionless parameters including width-depth ratio ($L = 2b/h$) and aspect ratio ($R_s = a/b$) are introduced. Two dimensionless variables $E_{h\omega n}$ and $ECOM_{\omega n}$ are introduced to represent the effect of hydrodynamic pressure and water compressibility on the natural frequency of the cylinders surrounded by water, which can be expressed as

$$E_{h\omega n} = \frac{|\omega_c - \omega_0|}{\omega_c} \times 100\% \tag{48}$$

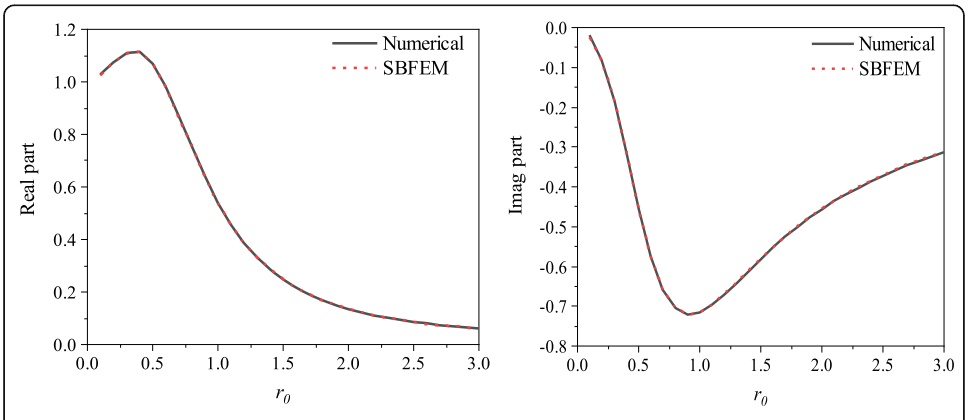

Fig. 5 The hydrodynamic pressure on the rigid elliptical cylinder in frequency

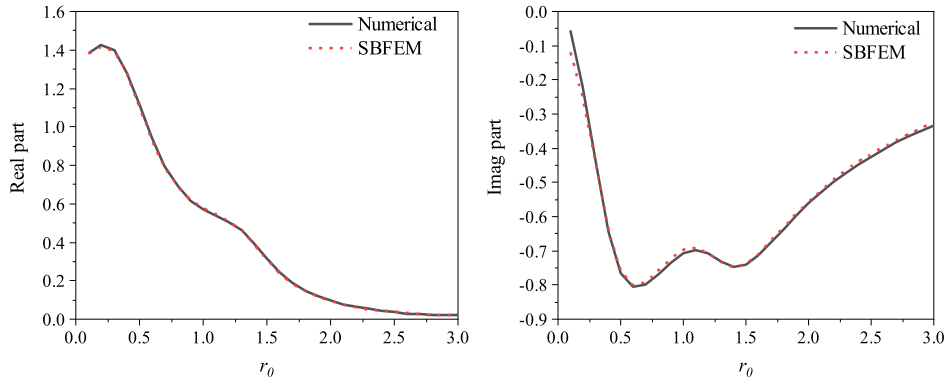

Fig. 6 The hydrodynamic pressure on the rigid rectangle cylinder in frequency

$$ECOM_{\omega n} = \frac{|\omega_c - \omega_i|}{\omega_c} \times 100\% \tag{49}$$

where, ω_c, ω_i and ω_0 mean the fundamental frequency of the cylinder surrounding by compressible water, incompressible water, and air, respectively.

The frequency responses of circular cylinders are firstly calculated, where the maximum displacement response on the top of the cylinder is selected as the observe

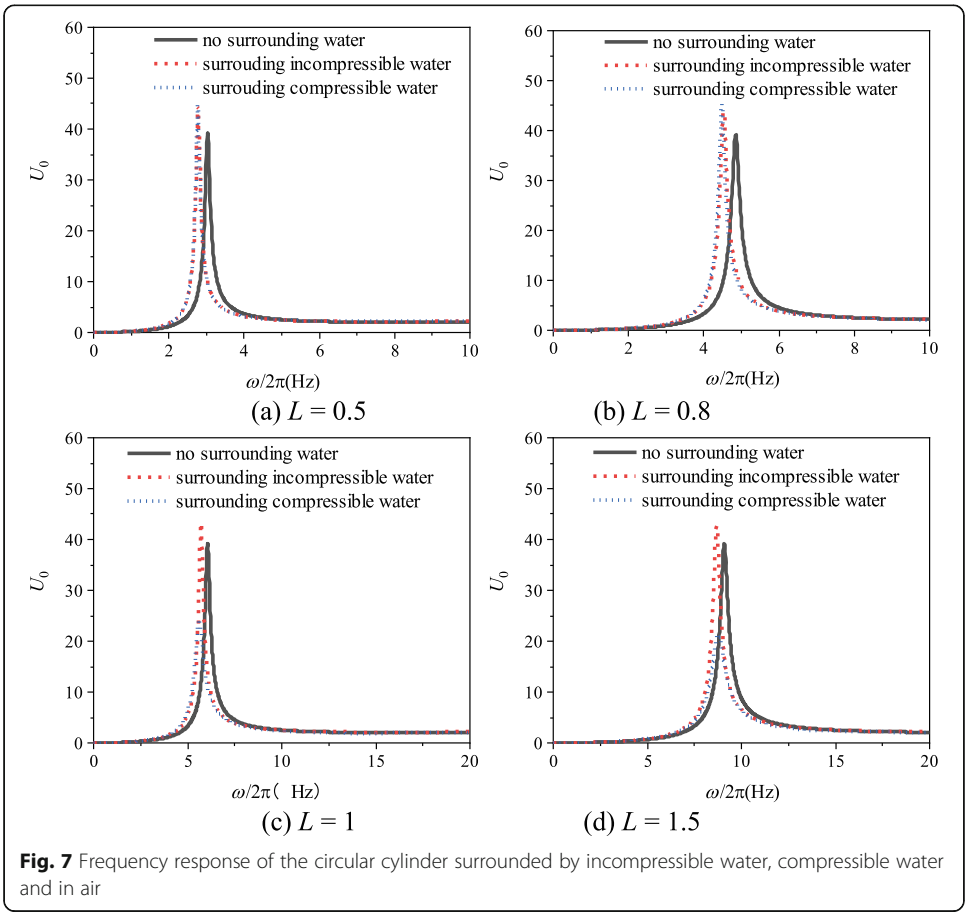

Fig. 7 Frequency response of the circular cylinder surrounded by incompressible water, compressible water and in air

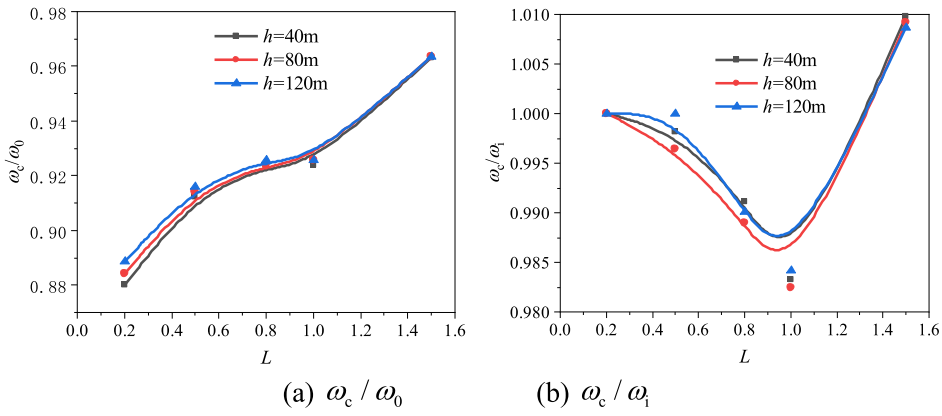

Fig. 8 Variation of the ratios ω_c/ω_0 and ω_c/ω_i with respect to L of circular cylinder

object. Figure 7 is the frequency response of the circular cylinder surrounded by incompressible water, compressible water and in air. Figure 8 shows the variation of the ratios ω_c/ω_0 and ω_c/ω_i with respect to L. It can be seen from Figs. 7 and 8 that water-cylinder interaction reduces the natural frequency of the cylinder, and this influence decreases as width-depth ratio increasing. It is obvious that water compressibility has little influence on the natural frequency of cylinder. Figure 9 shows the variation of the ratios Ac/An and Ac/Ai with respect to L, where Ac, Ai and An are the amplitude displacement on the top of cylinder at fundamental frequency in the case of compressible water, incompressible water and air. Compared Figs. 7 and 9, it can be seen that water-cylinder interaction can increase the seismic response of slender cylinders (circular cylinder $L \le 0.8$). However, water-cylinder interaction can significantly decrease the seismic response of squat cylinders (circular cylinder $L \ge 1$), and this trend increases as width-depth ratio increasing.

Figure 10 shows the variation of $E_{h\omega n}$ with respect to L for the elliptical and rectangle cylinders with different R_s. It is obvious that the effect of hydrodynamic pressure on the natural frequency decreases as L and R_s increase. Figure 11 shows the variation of

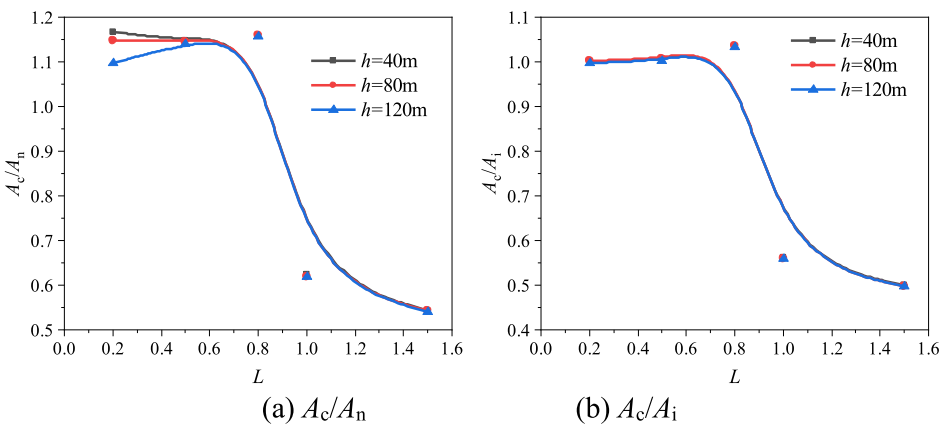

Fig. 9 Variation of the ratios A_c/A_n and A_c/A_i with respect to L of circular cylinders

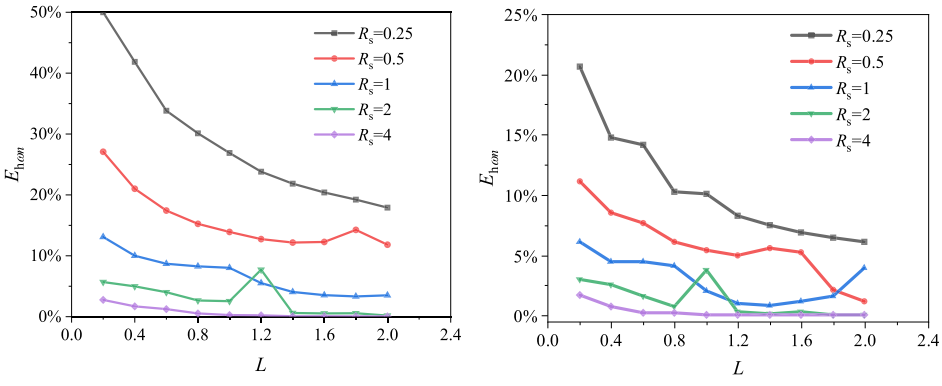

Fig. 10 Variation of $E_{h\omega n}$ with L for elliptical and rectangle cylinders

$ECOM_{\omega n}$ with respect to L for the elliptical and rectangle cylinders with different Rs. It can be seen that the effect of water compressibility decreases as L increases and this influence is limited in 6% for elliptical and rectangle cylinders with $L \le 2$ and $Rs \le 4$. In case of $L = 1.2$ and $R_s = 2$ ($L = 1.0$ and $R_s = 2$), the natural frequency of structure and surrounded by water is nearly resonance. Therefore, the effect of hydrodynamic pressure is significant, as shown in Fig. 10.

6 Conclusion

Based on the scaled boundary finite element, an accurate frequency domain model is proposed to simulate the seismic response of cylinders with arbitrary shapes cross-section surrounded by water. The numerical examples show that the proposed model has high-accuracy. The proposed model is also used to investigate the seismic responses and natural frequencies of the circular, elliptical and rectangle cylinders. The results indicate that water-cylinder interaction can reduces the natural frequency of the cylinder, and this influence decreases as width-depth ratio and aspect ratio increase. It

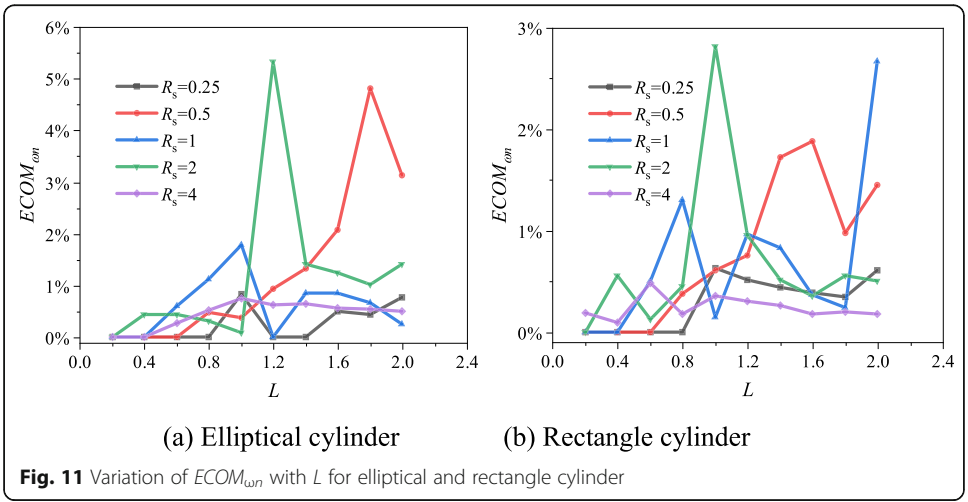

Fig. 11 Variation of $ECOM_{\omega n}$ with L for elliptical and rectangle cylinder

is also obtained that water compressibility has little influence on the natural frequency of cylinder.

7 Nomenclature

$P(x, y, z, \omega)$ hydrodynamic pressure expressed in frequency domain
ω circle frequency
c velocity of the wave propagate in water
$P_j(x, y, \omega)$ the modal hydrodynamic pressure in xy-plane
$\mathbf{N}$ mapping function
$\mathbf{J}$ Jacobi matrix

Acknowledgements
The support is gratefully acknowledged. The results and conclusions presented are of the authors and do not necessarily reflect the view of the sponsors.

Authors' contributions
MZ carried out the manuscript writing and numerical analysis, PW provided guidance in methodology development, PW and XW provided guidance in technical writing, PW, XW and CZ carried out the analytical model, and XD participated in the design of the study. The authors read and approved the final manuscript.

Funding
This work is supported by the National Natural Science Foundation of China (52078010) and Ministry of Education Innovation Team of China (IRT_17R03).

Availability of data and materials
All data, models, and code used during the study appear in the published article.

Competing interests
The author(s) declared no potential conflicts of interest with respect to the research, authorship, and/or publication of this article.

Received: 18 November 2020 Accepted: 13 December 2020
Published online: 08 January 2021

References

Avilés J, Li X (2001) Hydrodynamic pressures on axisymmetric offshore structures considering seabed flexibility. Comput Struct 79(29–30):2595–2606
Bazyar MH, Song C (2008) A continued-fraction-based high-order transmitting boundary for wave propagation in unbounded domains of arbitrary geometry. Int J Numer Methods Eng 74(2):209–237
Chandrupatla TR, Belegundu AD (2013) Introduction to finite elements in engineering, 4th edn. Pearson, Prentice Hall
Chen B-F (1997) 3d nonlinear hydrodynamic analysis of vertical cylinder during earthquakes. I: Rigid motion. J Eng Mech 123(5):458–465
Deeks AJ, Cheng L (2003) Potential flow around obstacles using the scaled boundary finite-element method. Int J Numer Methods Fluids 41(7):721–741
Deeks AJ, Wolf JP (2002) A virtual work derivation of the scaled boundary finite-element method for elastostatics. Comput Mech 28(6):489–504
Doherty JP, Deeks AJ (2005) Adaptive coupling of the finite-element and scaled boundary finite-element methods for non-linear analysis of unbounded media. Comput Geotech 32(6):436–444
Du X, Wang P, Zhao M (2014) Simplified formula of hydrodynamic pressure on circular bridge piers in the time domain. Ocean Eng 85(jul.15):44–53
Han RPS, Xu H (1996) A simple and accurate added mass model for hydrodynamic fluid—structure interaction analysis. J Frankl Inst 333(6):929–945
Jacobsen LS (1949) Impulsive hydrodynamics of fluid inside a cylindrical tank and of fluid surrounding a cylindrical pier. Bull Seismol Soc Am 39(3):189–204
Jiang H, Wang B, Bai X, Zeng C, Zhang H (2017) Simplified expression of hydrodynamic pressure on deepwater cylindrical bridge piers during earthquakes. J Bridg Eng 22(6):04017014
Li Q, Yang W (2013) An improved method of hydrodynamic pressure calculation for circular hollow piers in deep water under earthquake. Ocean Eng 72:241–256
Liao W (1986) Hydrodynamic interaction of flexible structures. J Waterw Port Coast Ocean Eng 111(4):719–731
Liaw CY, Chopra AK (1974) Dynamics of towers surrounded by water. Earthq Eng Struct Dyn 3(1):33–49
Meng XN, Zou ZJ (2012) Wave interaction with a uniform porous cylinder of arbitrary shape. Ocean Eng 44:90–99
Song C, Wolf JP (1996) Consistent infinitesimal finite-element cell method: three-dimensional vector wave equation. Int J Numer Methods Eng 39(13):2189–2208
Song C, Wolf JP (1997) The scaled boundary finite-element method—alias consistent infinitesimal finite-element cell method—for elastodynamics. Comput Methods Appl Mech Eng 147(3–4):329–355

Song C, Wolf JP (2002) Semi-analytical representation of stress singularities as occurring in cracks in anisotropic multi-materials with the scaled boundary finite-element method. Comput Struct 80(2):183–197
Song H, Tao L, Chakrabarti S (2010) Modelling of water wave interaction with multiple cylinders of arbitrary shape. J Comput Phys 229(5):1498–1513
Sun K, Nogami T (2010) Earthquake induced hydrodynamic pressure on axisymmetric offshore structures. Earthq Eng Struct Dyn 20(5):429–440
Tanaka Y, Hudspeth RT (1988) Restoring forces on vertical circular cylinders forced by earthquakes. Earthq Eng Struct Dyn 16(1):99–119
Ti Z et al (2020) Numerical approach of interaction between wave and flexible bridge pier with arbitrary cross section based on boundary element method. J Bridg Eng 25(11):4020095
Wang P, Zhao M, Du X (2018a) Analytical solution and simplified formula for earthquake induced hydrodynamic pressure on elliptical hollow cylinders in water. Ocean Eng 148(Jan.15):149–160
Wang P, Zhao M, Du X (2018b) Earthquake induced hydrodynamic pressure on a uniform vertical cylinder with arbitrary smooth cross-section. J Vib Shock 37(21):8–13 (In Chinese)
Wang P, Zhao M, Du X (2019a) A simple added mass model for simulating elliptical cylinder vibrating in water under earthquake action. Ocean Eng 179(May 1):351–360
Wang P, Zhao M, Du X (2019c) Simplified formula for earthquake-induced hydrodynamic pressure on round-ended and rectangular cylinders surrounded by water. J Eng Mech 145(2)
Wang P, Zhao M, Du X, Liu J, Chen J (2018d) Simplified evaluation of earthquake-induced hydrodynamic pressure on circular tapered cylinders surrounded by water. Ocean Eng 164(Sep.15):105–113
Wang P, Zhao M, Li H, Du X (2018c) An accurate and efficient time-domain model for simulating water-cylinder dynamic interaction during earthquakes. Eng Struct 166(Jul.1):263–273
Wang P, Zhao M, Li H, Du X (2019b) A high-accuracy cylindrical artificial boundary condition: water-cylinder interaction problem. Eng Mech 36(01):88–95 (In Chinese)
Wei K, Yuan W, Bouaanani N (2013) Experimental and numerical assessment of the three-dimensional modal dynamic response of bridge pile foundations submerged in water. J Bridg Eng 18(10):1032–1041
Westergaard HM (1933) Water pressures on dams during earthquakes. ASCE Trans 98:418–432
Williams AN (1986) Earthquake response of submerged circular cylinder. Ocean Eng 13:569–585
Woo-Sun P, Chung-Bang Y, Chong-Kun P (1991) Infinite elements for evaluation of hydrodynamic forces on offshore structures. Comput Struct 40(4):837–847
Zhao M, Li H, Du X, Wang P (2018) Time-domain stability of artificial boundary condition coupled with finite element for dynamic and wave problems in unbounded media. Int J Comput Methods 1850099

Publisher's Note